Cell
PRESS

Apoptosis Regulates ipRGC Spacing Necessary for Rods and Cones to Drive Circadian Photoentrainment

Shih-Kuo Chen,[1,7] Kylie S. Chew,[1,7] David S. McNeill,[1,7] Patrick W. Keeley,[2] Jennifer L. Ecker,[1] Buqing Q. Mao,[3] Johan Pahlberg,[3] Bright Kim,[4] Sammy C.S. Lee,[2] Michael A. Fox,[5] William Guido,[5] Kwoon Y. Wong,[4] Alapakkam P. Sampath,[3] Benjamin E. Reese,[2] Rejji Kuruvilla,[1,*] and Samer Hattar[1,6,*]

[1]Department of Biology, Johns Hopkins University, Baltimore, MD 21218, USA
[2]Neuroscience Research Institute and Departments of Psychological and Brain Sciences and Molecular, Cellular and Developmental Biology, University of California, Santa Barbara, Santa Barbara, CA 93106, USA
[3]Department of Physiology and Biophysics, Zilkha Neurogenetic Institute, University of Southern California Keck School of Medicine, Los Angeles, CA 90089, USA
[4]Department of Ophthalmology & Visual Sciences, University of Michigan, Ann Arbor, MI 48105, USA
[5]Department of Anatomy and Neurobiology, Virginia Commonwealth University, Richmond, VA 23298, USA
[6]The Solomon Snyder Department of Neuroscience, Johns Hopkins University School of Medicine, Baltimore, MD 21218, USA
[7]These authors contributed equally to this work
*Correspondence: rkuruvilla@jhu.edu (R.K.), shattar@jhu.edu (S.H.)
http://dx.doi.org/10.1016/j.neuron.2012.11.028

SUMMARY

The retina consists of ordered arrays of individual types of neurons for processing vision. Here, we show that such order is necessary for intrinsically photosensitive retinal ganglion cells (ipRGCs) to function as irradiance detectors. We found that during development, ipRGCs undergo proximity-dependent Bax-mediated apoptosis. *Bax* mutant mice exhibit disrupted ipRGC spacing and dendritic stratification with an increase in abnormally localized synapses. ipRGCs are the sole conduit for light input to circadian photoentrainment, and either their melanopsin-based photosensitivity or ability to relay rod/cone input is sufficient for circadian photoentrainment. Remarkably, the disrupted ipRGC spacing does not affect melanopsin-based circadian photoentrainment but severely impairs rod/cone-driven photoentrainment. We demonstrate reduced rod/cone-driven cFos activation and electrophysiological responses in ipRGCs, suggesting that impaired synaptic input to ipRGCs underlies the photoentrainment deficits. Thus, for irradiance detection, developmental apoptosis is necessary for the spacing and connectivity of ipRGCs that underlie their functioning within a neural network.

INTRODUCTION

The retina detects and processes light information such as intensity, contrast, color, and motion before conveying it to the brain. To precisely convey the spatial mapping of these visual qualities, many different types of neurons form regularly spaced arrays across the surface of the retina (Cook and Chalupa, 2000). Yet how each type of neuron forms such an ordered distribution, which occurs during development, is an area of emerging interest (Reese, 2008). In the vertebrate retina, it has been shown that mosaics form through different developmental processes including periodic fate assignment, tangential dispersion, or apoptosis (Galli-Resta, 2002). Similar to other neuronal populations, more than half of the retinal ganglion cells (RGCs) are eliminated during development by apoptosis (Perry et al., 1983; Mosinger Ogilvie et al., 1998; Farah and Easter, 2005). Deletion of Bax, a proapoptotic factor, prevents this loss of RGCs (Mosinger Ogilvie et al., 1998). Although apoptosis mediated through Bcl-2 family members including Bax contributes to the spatial distribution of some retinal cell types (Raven et al., 2003; Keeley et al., 2012), there has been no direct demonstration of any functional consequences associated with such disrupted cell spacing, specifically, upon retinal circuitry and behavior.

Similar to other retinal cell types, the subtypes of intrinsically photosensitive RGCs (ipRGCs) form independent mosaics across the retina (Berson et al., 2010). We have previously developed several genetically modified mouse models that allow us to specifically label ipRGCs as well as quantitative behavioral assays that permit an assessment of their functional output (Hattar et al., 2002; Güler et al., 2008; Ecker et al., 2010). Using a variety of spatial statistics to ascertain the regularity and intercellular spacing of such mosaics, in conjunction with the above anatomical and functional tools, we have examined the role of apoptosis in generating a cell-type-specific mosaic and its behavioral significance.

ipRGCs are the sole conduit for light information to influence several distinct behavioral outputs. Their axons target the suprachiasmatic nucleus (SCN) for photoentrainment of circadian rhythms and the olivary pretectal nucleus (OPN) for pupillary light responses (PLR) (Hattar et al., 2002; Hattar et al., 2006; Güler et al., 2008). Unlike other types of RGCs, the ipRGCs combine their intrinsic melanopsin-based photosensitivity with extrinsic
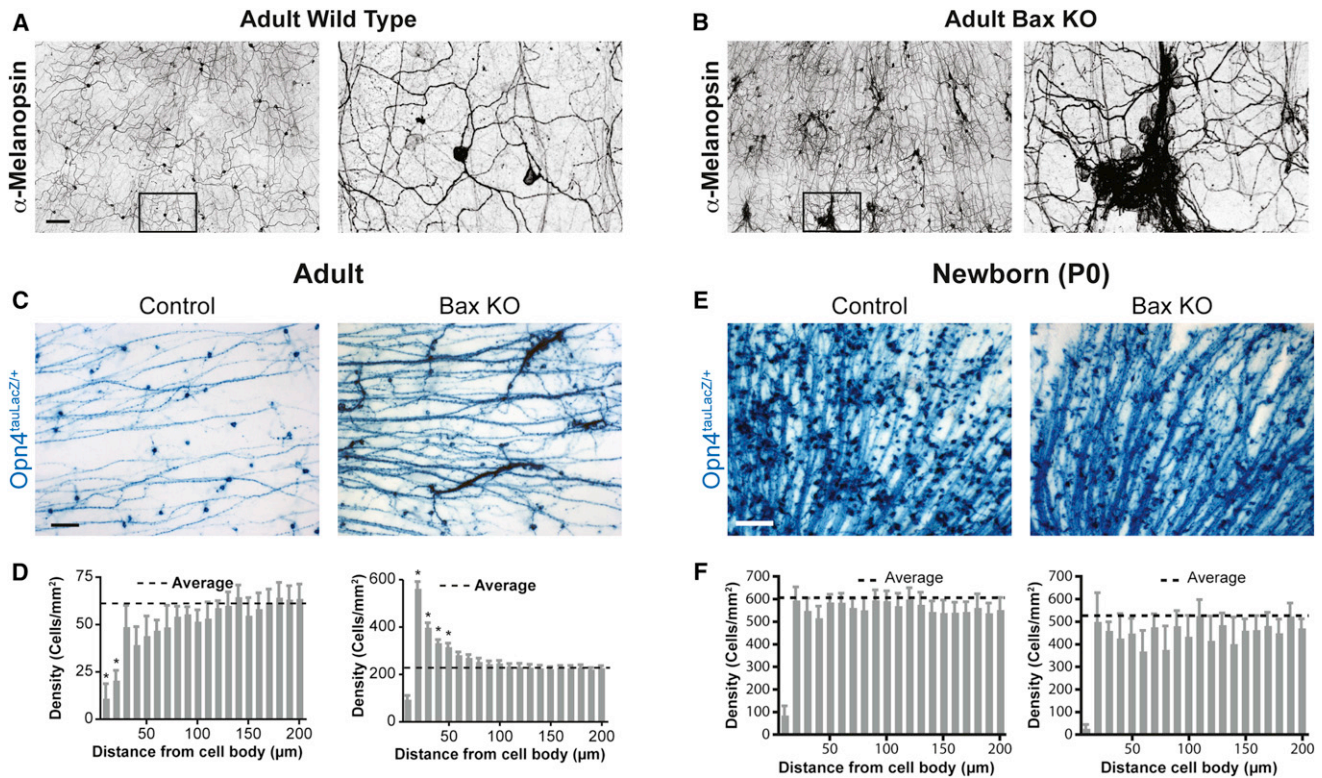
Figure 1. Bax Is Required for Correct Spacing of ipRGCs

Melanopsin immunofluorescence on whole-mount retinas from adult mice (A and B). In control wild-type mice (A), the ipRGC dendrites form a receptive net across the retina. The *Bax* knockout (*Bax* KO) contains clusters of ipRGCs (B) with fasciculated dendrites.

(C) X-gal staining of M1 ipRGCs, which preferentially labels somata and axons, in whole-mount retinas from control and *Bax* KO adult mice.

(D) Density recovery profiles derived from the autocorrelation from images such as those in (C) show that ipRGCs form a spaced distribution in the control (lower than average density in bins closer to the origin) and a clustered distribution in the *Bax* KO (higher than average density in bins closer to the origin; n = 6 retinas for each group). Note that the closest bin is always lower than average since the cell body size prevents most cells from being closer than 10 μm to each other.

(E) X-gal staining of M1 ipRGCs in whole-mount retinas from control (*Bax*$^{+/-}$) and *Bax* KO littermate mice at P0. (F) Density recovery profiles for ipRGCs from control and *Bax* KO mice at P0 shows a random distribution of ipRGCs at this time for both groups (average density in all bins except the closest; n = 5 retinas for each group).

Data are mean ± SEM; scale bars are 100 μm; * indicates significance from the average density by one-way ANOVA with Tukey post hoc, p < 0.05, mean ± SEM.

input from rods and cones (Mrosovsky and Hattar, 2003). Either the extrinsic rod/cone signal or the intrinsic melanopsin-based signal is sufficient to drive both photoentrainment and PLR (Freedman et al., 1999; Lucas et al., 2001; Panda et al., 2002; Ruby et al., 2002; Hattar et al., 2003a; Lucas et al., 2003). Thus, in melanopsin knockout animals, the rod/cone input to ipRGCs can be assessed at the behavioral level independent of the intrinsic light response. Here, we determined the role of apoptosis in generating the spatial distribution, connectivity and functional output of ipRGCs using *Bax* mutant mice. We show that Bax-mediated apoptosis, in both germline and ipRGC-specific *Bax* mutant mice, is required to establish a spaced mosaic of ipRGCs during development. Disruption of the spaced distribution of ipRGCs does not impair functional responses driven by the intrinsic photosensitivity of ipRGCs in *Bax* mutant mice. However, rod/cone signaling through ipRGCs to drive circadian photoentrainment is severely attenuated, consistent with anatomical and physiological evidence for disrupted rod/cone activation of ipRGCs. Thus, for irradiance

detection, developmental apoptosis is necessary for the spacing and connectivity of ipRGCs that underlie their functioning as a component of a neural network without affecting their role as intrinsic light sensors.

RESULTS

Bax-Dependent Apoptosis Mediates Formation of the ipRGC Mosaic

Melanopsin immunofluorescence on whole-mount retinas from adult wild-type and *Bax* knockout (*Bax*$^{-/-}$) mice reveals that ipRGCs in *Bax*$^{-/-}$ mice form clumps with highly fasciculated dendrites (Figures 1A and 1B; see Table S1 available online), similar to the clustering recently described in the Dscam mutant retina (Fuerst et al., 2009; Keeley et al., 2012). The clustering observed in the *Bax*$^{-/-}$ mice is not informative about single type of retinal neuron, since recent evidence demonstrates that ipRGCs comprise multiple subtypes (Provencio et al., 2002; Viney et al., 2007; Baver et al., 2008; Schmidt and Kofuji,
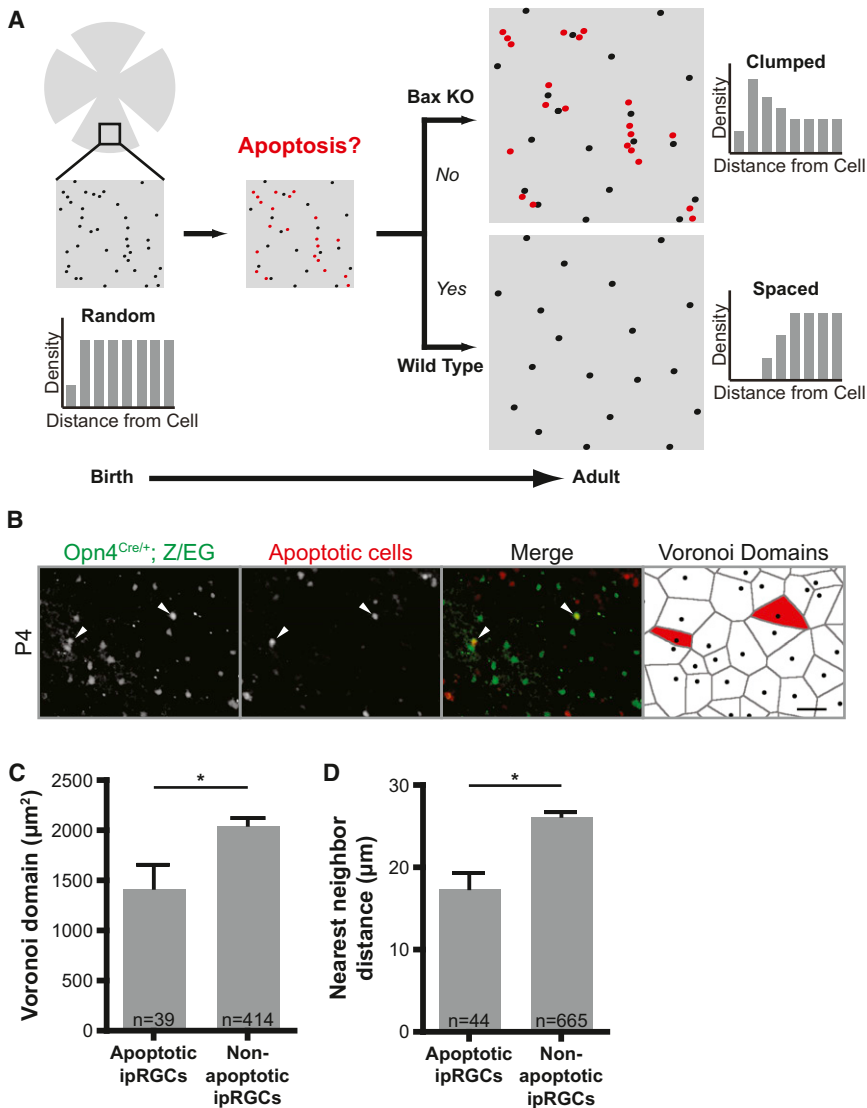
Figure 2. Proximity-Based Apoptosis Leads to Proper ipRGC Spacing

(A) Model showing how proximity-based apoptosis may generate a mosaic for a specific cell type. Only cell positioning, not fasciculation, is shown, for clarity. Cells in close proximity to each other (shown in red) are eliminated by Bax-mediated apoptosis to form a more spaced distribution in the adult. In *Bax* KO mice, cells in close proximity to each other survive.

(B) Total ipRGCs were labeled in green at P4 with an anti-GFP antibody in *Opn4*[Cre/+]*; Z/EG* mice. Cells undergoing apoptosis were stained red by TUNEL and two antibodies specific for activated caspase-3 and activated Bax. Apoptotic ipRGCs (positive for any of these three indicators of cell death) are indicated with arrowheads (scale bar 50 μm). The last panel shows Voronoi domains (VD) for each ipRGC in the field, with the VD for the dying ipRGCs labeled in red.

(C) The subset of ipRGCs undergoing apoptosis at P4 have significantly smaller Voronoi domains than nonapoptotic ipRGCs (1429 ± 230.5 μm^2, n = 39 for apoptotic; 2059 ± 66.95, n = 414 for nonapoptotic, from eight retinas; p = 0.0062 by Student t test, mean ± SEM).

(D) The apoptotic ipRGCs had a significantly smaller nearest neighbor distance to adjacent ipRGCs than nonapoptotic ones (17.49 ± 1.848 μm, n = 44 for apoptotic; 26.28 ± 0.4741 μm, n = 665 for nonapoptotic, from eight retinas; p < 0.0001 by Student t test, mean ± SEM).

We found a significant depletion of ipRGCs between P3 and P9 (Figure S1), which is in agreement with both the timing and the magnitude of developmental apoptosis for the conventional RGCs (Dreher et al., 1983; Perry et al., 1983).

To objectively demonstrate the clumping phenotype observed in M1 ipRGCs of *Bax* mutants (Figure 1C), we performed autocorrelation analysis in control mice and showed that M1 ipRGCs form a spaced distribution across the retina by forming an average exclusion zone of ~40 μm around each ipRGC soma (Figure 1D, left panel), a defining trait of retinal mosaics (Cook, 1998). In contrast, in *Bax* mutant mice, we noted that M1 ipRGC somata failed to exhibit normal exclusion zones and instead showed a clustering of ipRGC cell bodies, confirming the disruption in cell spacing for a single class of ipRGC (Figure 1D, right panel). Consistent with a role for cell death in the spacing of ipRGCs, at P0, a time point preceding cell death, control and *Bax*^{−/−} mice have similar average densities of M1 ipRGCs and both show a random distribution of them (i.e., one that is neither spaced nor clustered) (Figures 1E and 1F). These results indicate that ipRGCs are first generated in a random distribution, and then progress to either a spaced distribution in the wild-type or a clumped distribution in *Bax*^{−/−} mice.

These results suggest a model by which proximity between neighboring cells promotes apoptosis (Figure 2A), and loss of

2009; Ecker et al., 2010), of which, several form individual mosaics (Berson et al., 2010). To better study ipRGC mosaic formation, we analyzed one single subtype, the M1 ipRGCs, which are labeled by X-gal staining in the *Opn4*[tauLacZ] reporter mice (Figure 1C; Table S1; Hattar et al., 2002; Baver et al., 2008). In *Bax*^{−/−} mice, we found a 3.7-fold higher average density of ipRGCs than in the controls (Figure 1D). No changes in total retinal area were observed between *Bax*^{−/−} and wild-type animals (data not shown). This increase in ipRGC density indicates that similar to other RGCs, ipRGCs also undergo Bax-mediated apoptosis during development (Mosinger Ogilvie et al., 1998; White et al., 1998). To determine the developmental stage at which ipRGCs undergo apoptosis, we used the *Opn4*[Cre/+] animals in conjunction with the *Z/AP* reporter allele (Lobe et al., 1999; Ecker et al., 2010) to permanently label all ipRGC subtypes with alkaline phosphatase (AP) (Table S1). In the *Opn4*[Cre/+]*; Z/AP* animals, any decrease in the numbers of AP labeled cells during development should be due to apoptosis.
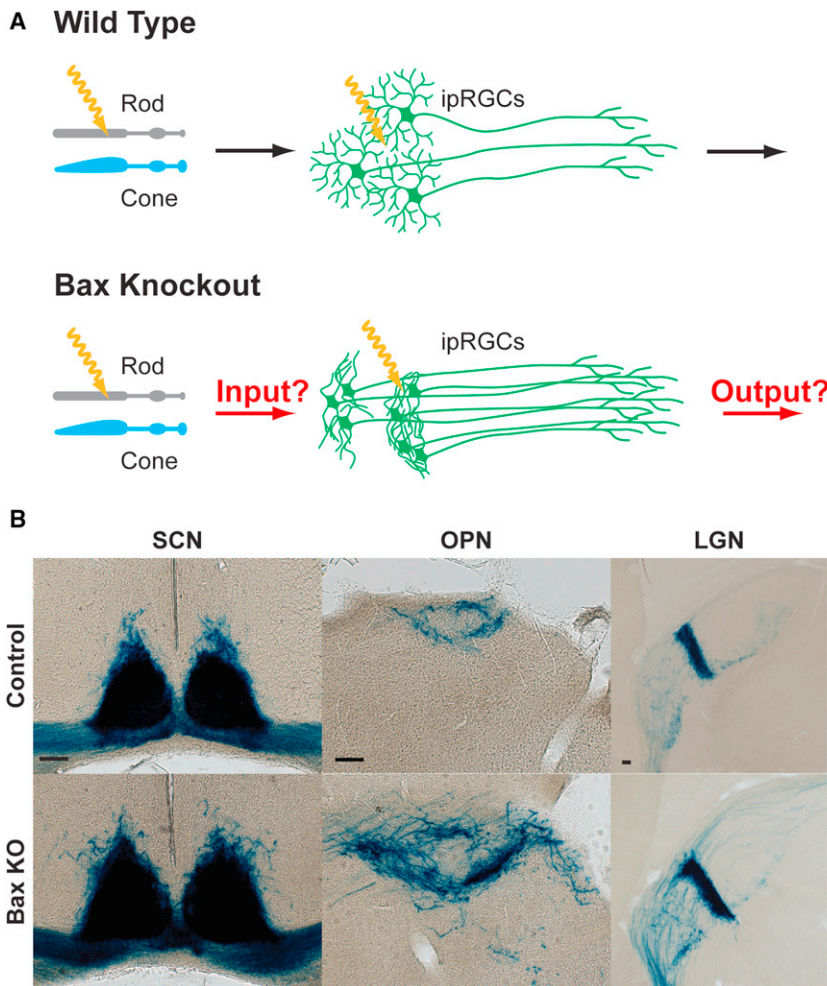
Figure 3. Axonal Targeting Remains in *Bax* Knockout

(A) Model describing how lack of apoptosis in ipRGCs might affect reception of light information from rods and cones, and/or transmission of light information to downstream nuclei in the brain.

(B) Axons from ipRGCs were labeled by X-gal staining with the *Opn4^tau-LacZ* reporter allele in coronal sections of the SCN (left panel), OPN (middle panel), and IGL (right panel). ipRGC axons still confine to the SCN, OPN, and IGL in the *Bax* KO similar to the control (scale bar, 100 μm).

form the distribution of ipRGCs from random into spaced (Figure 2A).

Bax Is Crucial for ipRGC Connection to Upstream Retinal Circuitry

We next sought to determine if the clumped ipRGC distribution in the *Bax* mutants affect the ability of ipRGCs to mediate non-image-forming functions (Figure 3A). We first wanted to ensure whether ipRGC axons exhibit normal innervation of their brain targets in the *Bax* mutants. To assess M1 ipRGC axonal targeting, we used X-gal staining in coronal brain sections from *Bax^−/−* mice also harboring the *Opn4^tau-LacZ* reporter allele (*Opn4^tau-LacZ/+*; *Bax^−/−*; Table S1; Hattar et al., 2002). *Opn4^tau-LacZ/+* animals were used as controls. Despite altered M1 ipRGC spacing and fasciculated dendritic morphology in *Bax* mutant animals, we observed normal axonal targeting in the major retinorecipient brain regions of M1 ipRGCs, such as the suprachiasmatic nucleus (SCN) and intergeniculate leaflet (IGL), responsible for circadian rhythms, and the shell of the olivary pretectal nucleus, a relay center for the pupillary light reflex (Figure 3B). Although we observed denser innervation in *Bax* mutant animals, likely due to increased ipRGC numbers, we did not observe any navigational errors or ectopic ipRGC innervation in central brain targets (Figures 3B and S2).

A longstanding view in the circadian field is that the radiating dendritic arbors of spaced ipRGCs are necessary to form an evenly distributed receptive net in order to increase the area for photon capture to allow photoentrainment (Provencio et al., 2002). Given the disrupted features of the ipRGC mosaic in *Bax* mutants, we tested circadian photoentrainment using wheel-running activity. Surprisingly, *Bax* mutant animals are able to photoentrain to a 12 hr:12 hr light-dark cycle similar to controls (Figures 4A and 4B; wild-type and *Bax* KO). The mutants had similar circadian period length to wild-type animals (Figures 4A and 4C), and presenting a single pulse of light of 15 min duration caused similar phase shifts in the *Bax* mutant and control mice (Figures 4A and 4D). In addition, exposing the
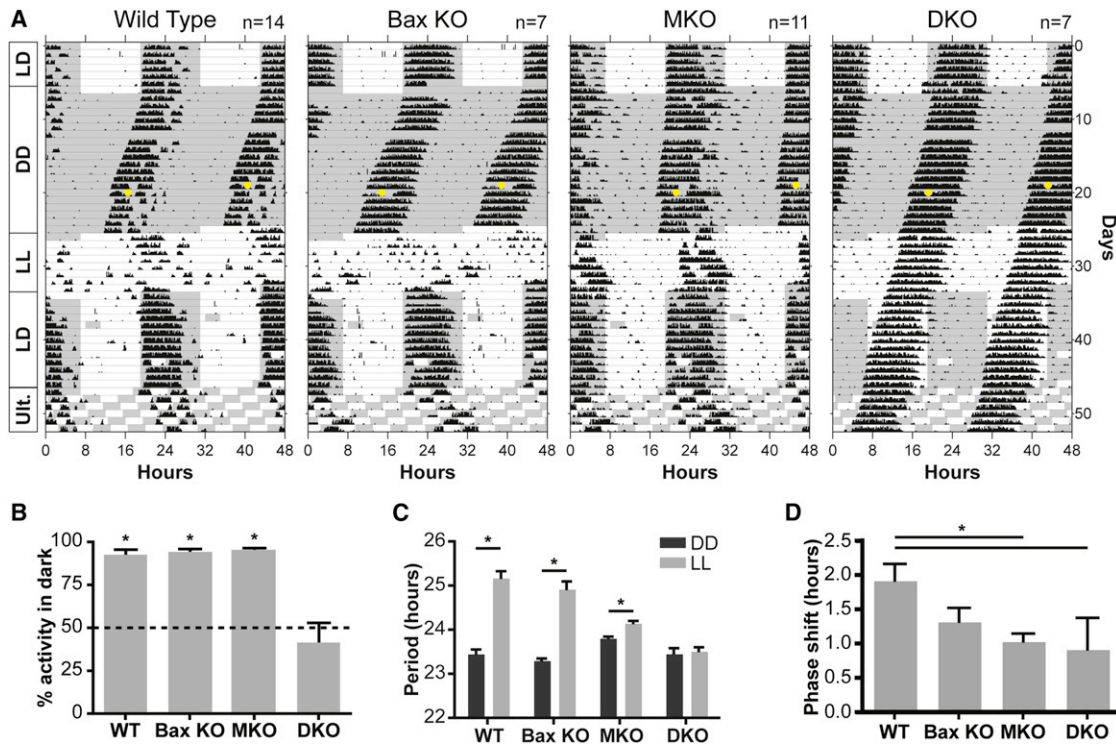
Bax abrogates this proximity-based effect. To test this model, we determined the spatial relationship between dying cells and their immediate neighbors. Since apoptotic cells are believed to be present for only ~1 hr (Cellerino et al., 2000), we combined three different labels for apoptotic cells (TUNEL and two antibodies specific for activated caspase-3 and activated Bax) to increase our chances of finding ipRGCs that were undergoing apoptosis. The latter were detected by using the *Z/EG* reporter line (Novak et al., 2000) to fluorescently label ipRGCs (Table S1). ipRGCs comprise 2% of RGCs, and we found only 77 ipRGCs undergoing apoptosis in eight retinas (Figure 2B). For each of those cells, we performed Voronoi domain (VD) analysis (Figure 2B, right panel) followed by nearest neighbor measurements. The Voronoi domain of a cell defines the area surrounding the cell containing all points closer to that cell than to any other cell. The closest of those Voronoi neighbors is the nearest neighbor. We found that apoptotic ipRGCs had significantly smaller Voronoi domains and shorter nearest neighbor distances than viable ipRGCs (Figures 2C and 2D). These results suggest that ipRGCs that are in close proximity preferentially undergo apoptosis. Proximity-based apoptosis may thereby generate exclusion zones that trans-

Figure 4. Rod/Cone Input to ipRGCs Is Highly Attenuated in *Bax* Knockout Mice

(A) Wheel-running actograms from wild-type (WT), *Bax* KO, *Opn4* KO (MKO), and *Bax/Opn4* double KO (DKO) mice. Only DKO mice were unable to entrain their activity to different light cycles: 12:12 hr light:dark (LD), constant darkness (DD), constant light (LL), and ultradian cycle (3.5:3.5 hr light:dark). The gray background denotes when lights were off.

(B) DKO mice were unable to confine their activity to the dark portion of the 12:12 LD cycle in (A), as indicated by no significant difference from 50% (t test, * indicates p < 0.05).

(C) DKO mice did not lengthen their period under constant light (paired t test, * indicates p < 0.05).

(D) A 15 min light pulse at CT16 (circles in B) generated a similar phase shift in all groups of mice (no significant difference by one-way ANOVA with Tukey post hoc).

For all graphs, mean ± SEM.

animals to constant light (LL), wild-type and *Bax* mutants show similar lengthened circadian periods compared to constant darkness (Figures 4A and 4C). Finally, the wild-type and *Bax* mutant mice can fully re-entrain to a 24 hr light-dark cycle and mask under a 3 hr light pulse or under a 7 hr (ultradian) light-dark cycle (Figure 4A). Together, these behavioral studies indicate that *Bax* mutants were able to respond to various circadian light paradigms indistinguishably from wild-type mice (Figures 4A, left two panels, and 4B–4D). This indicates that the loss of apoptosis, the disrupted cellular spacing and the altered dendritic morphologies in *Bax* mutants do not impair the output of light signals from ipRGCs to the brain as revealed by several light-dependent circadian functions (Figure 3).

We next sought to determine if the disrupted mosaic features in the *Bax*$^{-/-}$ mice would affect the ability of ipRGCs to receive light input originating from rods and cones. We show that electroretinograms (ERGs) from the *Bax*$^{-/-}$ animals are indistinguishable from wild-type animals (Figure S3A), indicating that the *Bax* deletion does not alter outer retinal signaling between the classical photoreceptor rods and cones and their immediate synaptic partners. In addition, *Bax* mutants are able

to visually locate a platform in the Morris water maze similar to wild-type animals (Figure S3B). To test the extrinsic rod/cone input to ipRGCs in the context of the *Bax* deletion, we eliminated the intrinsic melanopsin-based photoreception (*Opn4*$^{tau-LacZ/tau-LacZ}$, referred to here as *Opn4*$^{-/-}$; Table S1) in *Bax*$^{-/-}$ mice and subjected the double knockout animals (*Bax*$^{-/-}$; *Opn4*$^{-/-}$) to the same circadian light paradigms as above (Figure 4A; Table S1; DKO). As a control, we used the *Opn4*$^{-/-}$ mice (MKO). As previously demonstrated, the *Opn4*$^{-/-}$ mice are able to photoentrain, but show attenuated period lengthening in LL and a decrease in phase shifting magnitude in response to light (Figures 4A and 4D; MKO; Panda et al., 2002; Ruby et al., 2002). The ability of the *Opn4*$^{-/-}$ mice to photoentrain indicates that ipRGCs rely on the extrinsic input from rods and cones to convey light information for photoentrainment in the absence of the melanopsin protein. In contrast to the *Opn4*$^{-/-}$ mice, photoentrainment was severely impaired in all *Bax*$^{-/-}$; *Opn4*$^{-/-}$ (DKO) mice (Figure 4A, right panel). The majority of *Bax*$^{-/-}$; *Opn4*$^{-/-}$ mice free-ran regardless of the light-dark cycle (Figure S4), showing equal amounts of activity (~50%) in the light and dark portions of the cycle (Figure 4B).
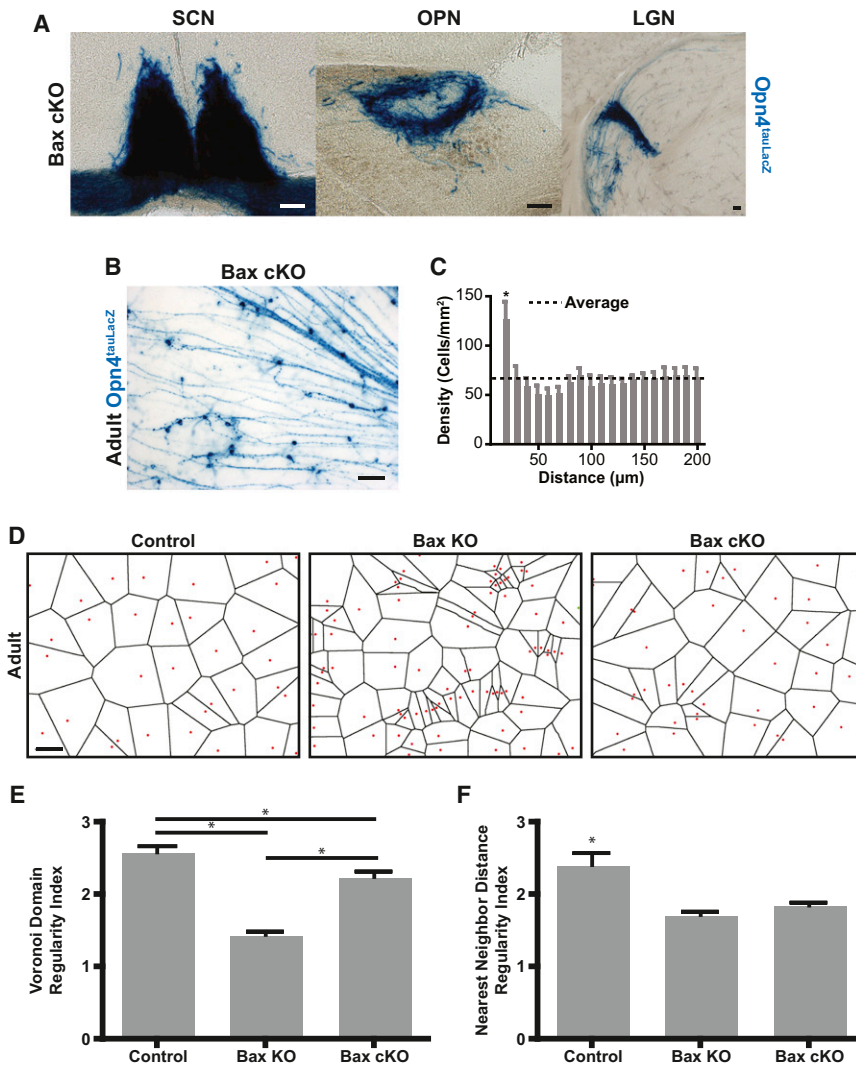
2005; Ecker et al., 2010) and show normal axonal targeting of ipRGCs to the brain (Figure 5A). Autocorrelation analysis in the *Bax^fl/fl; Opn4^Cre/tau-LacZ* (Table S1) mice show deficits in ipRGC spacing similar to those seen in the conventional *Bax^−/−* retina (Figures 5B and 5C; compare with Figures 1C and 1D, right panels). In contrast to *Bax^−/−* animals, however, ipRGC dendrites from the *Bax^fl/fl; Opn4^Cre/tau-LacZ* animals were not fasciculated (Figure 5B) and ipRGC cell density was similar to wild-type animals (Figures 5B and 5C; compare with Figures 1C and 1D, left panels). These milder phenotypes are likely due to the inefficient deletion of *Bax* by the melanopsin-driven Cre recombinase. Consistent with this hypothesis, Bax antibody staining in conditional *Bax* mutants shows residual Bax immunoreactivity in some melanopsin cells compared to the conventional *Bax* mutants where no Bax staining is seen (Figure S5A). In addition, using *Math5^Cre/+*, where Cre driven deletion of *Bax* occurs at an earlier developmental point than in the *Bax^fl/fl; Opn4^Cre/+* mice (Yang et al., 2003; McNeill et al., 2011), we show the increase in cell numbers and the fasciculated dendritic morphologies observed in the conventional *Bax* mutants (Figure S5B). However, even without increased cell number and fasciculated dendrites, the conditional *Bax^−/−* mice show deficits in cell spacing evidenced by autocorrelation analysis (Figure 5C). We further determined that in *Bax^fl/fl; Opn4^Cre/+* mice, loss of the minimal spacing between neighboring cells manifests itself as a less regular

This behavior is comparable to the free-running response seen in mice lacking rod, cone and ipRGC phototransduction pathways (*Gnat1^−/−*; *Cnga3^−/−*; *Opn4^−/−*, referred to here as triple KO animals) (Hattar et al., 2003b). Similar to the triple KO animals, *Bax^-/-*; *Opn4^−/−* mice were also unable to lengthen their period in constant light (Figure 4C). Thus, loss of Bax disrupts the ability of ipRGCs to receive extrinsic input from rods and cones. However, in contrast to the triple KO mice, the *Bax^−/−*; *Opn4^−/−* mice retain a limited capacity to respond to rod/cone input; the *Bax^−/−*; *Opn4^−/−* mice still show a similar phase-shift as *Opn4^−/−* mice in response to a 15 min light pulse (Figure 4D). These results show that the loss of Bax perturbs the rod/cone input to circadian photoentrainment.

Since the *Bax* deletion in the conventional knockouts may affect all retinal cell types in addition to ipRGCs (White et al., 1998), we employed a conditional approach to test the cell autonomous role of Bax in ipRGCs. We conditionally deleted *Bax* in ipRGCs by mating *Opn4^Cre* mice with animals harboring a floxed *Bax* allele (*Bax^fl/fl; Opn4^Cre/+*; Table S1; Takeuchi et al.,
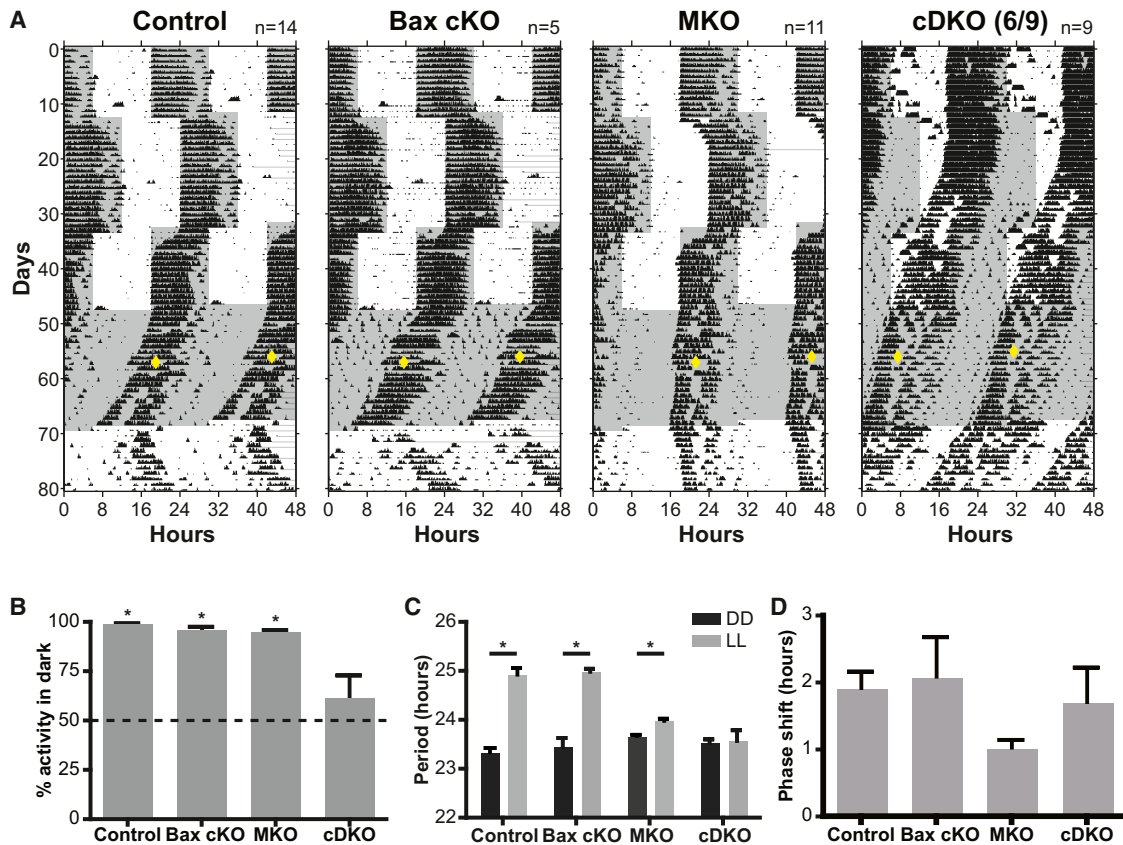
Figure 6. Conditional *Bax* Knockout in ipRGCs Attenuates Rod/Cone Input

(A) Wheel-running actograms from control, *Bax* conditional knockout (*Bax* cKO), *Opn4* KO (MKO), and *Bax* conditional/*Opn4* double-KO mice (cDKO). The majority of cDKO mice (6 out of 9) show significant deficits in their responses to different light cycles: 12:12 hr light:dark (LD) with 6 hr phase delay and advance, constant darkness (DD), and constant light (LL). The gray background denotes when lights were off.

(B) cDKO mice were unable to confine their activity to the dark portion of the 12:12 LD cycle in (A), as indicated by no significant difference from 50%.

(C) cDKO mice did not lengthen their period under constant light.

(D) A 15 min light pulse at CT16 phase shift (diamonds in A) generated a similar phase shift in all groups of mice (* indicates p < 0.05 with a one-way ANOVA with Tukey post hoc, mean ± SEM).

mosaic, evidenced by both the Voronoi domain and nearest neighbor regularity indexes (Figures 5D–5F). The conditional mice show less of an effect upon their Voronoi domain regularity indexes compared to *Bax*$^{-/-}$ mice (Figures 5D and 5E), since their lower density rarely yields many close neighbors to generate very small domains. They do, however, show nearest neighbor regularity indexes similar to those in the *Bax*$^{-/-}$ retina.

We subsequently tested photoentrainment in the wild-type and conditional *Bax* mutants. As predicted from the conventional *Bax*$^{-/-}$ mice, the conditional *Bax*$^{-/-}$ shows normal circadian photoentrainment in the presence of melanopsin phototransduction pathway. Similar to *Bax*$^{-/-}$; *Opn4*$^{-/-}$ animals, the majority of mice lacking the melanopsin protein and Bax selectively in the ipRGCs (*Bax*$^{fl/fl}$; *Opn4*$^{Cre/tau-LacZ}$, cDKO) exhibited significant photoentrainment deficits with a subset showing a mild photoentrainment deficits (Figures 6 and S6). As expected, ERG recordings from the conditional *Bax* mutants showed no deficits in outer retinal circuitry (Figure S3A). These results show that even partial developmental deletion of Bax in

Bax$^{fl/fl}$; *Opn4*$^{Cre/tau-LacZ}$ mice is sufficient to disrupt the organization of M1 ipRGCs and cause circadian photoentrainment deficits.

Bax Mutant Mice Show Ectopic Retinal Lamination, an Increase in Ectopic Synapses within the Inner Nuclear Layer, and Impairments in Rod/Cone-Mediated Activation of ipRGCs

To assess the anatomical and physiological underpinnings of this disruption in rod/cone input to ipRGCs, we focused on *Bax* mutant mice because of the greater effects upon the organization of the ipRGC mosaic and the greater consistency in the behavioral deficits across *Bax* mutant mice. We first examined the dendritic architecture of ipRGCs in retinal sections. ipRGC dendritic arbors were frequently misplaced to ectopic locations within the middle of the inner nuclear layer (INL) (arrowheads in Figure 7A, bottom panels labeled green) spanning the whole retina (Figure S7). Coincident with such misplaced dendrites, an ectopic cell-sparse synaptic layer was observed to form
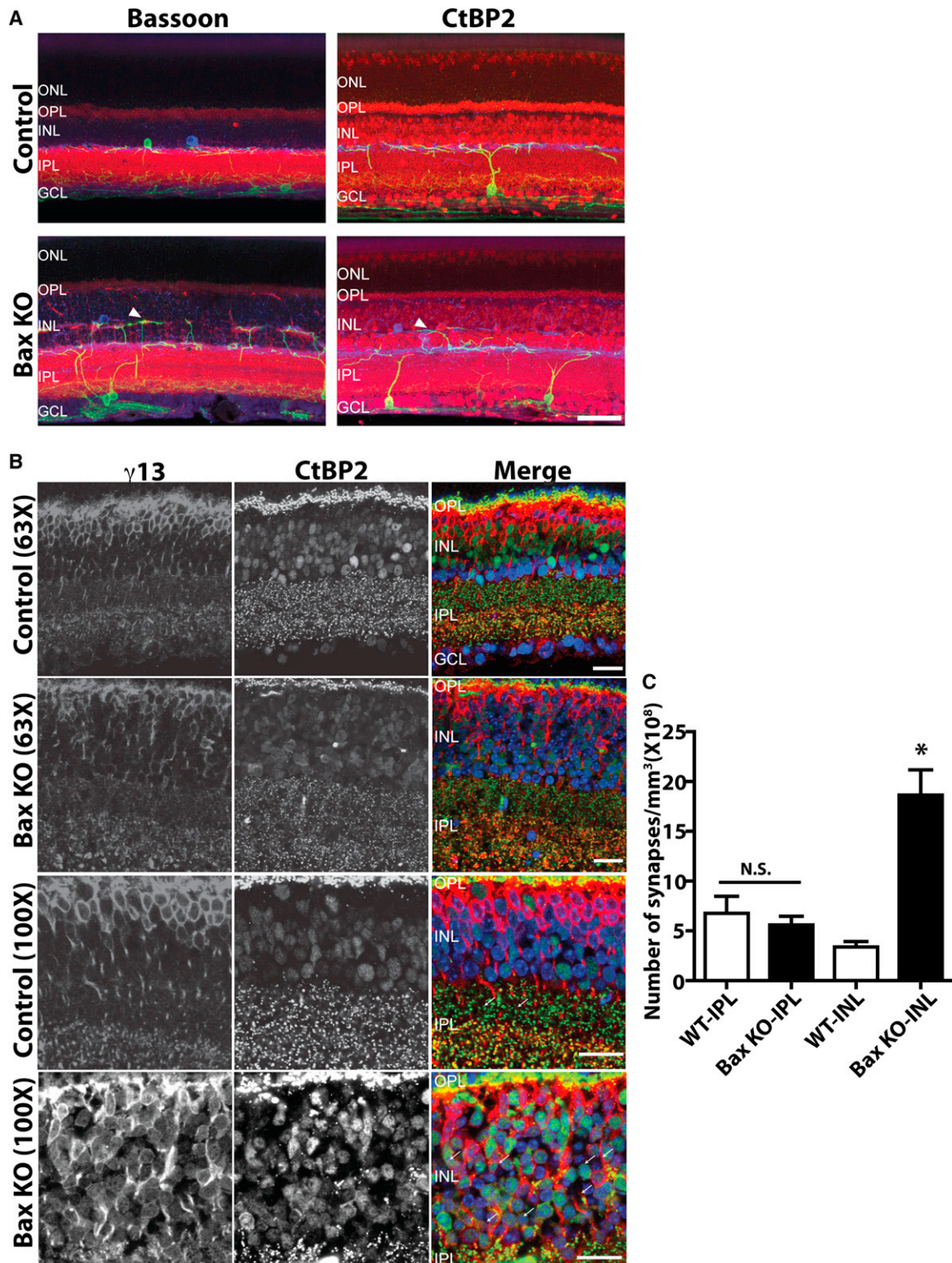
Figure 7. Altered Dendritic Morphology and Increased Ectopic Synapses in *Bax* Knockout Mice

(A) Immunofluorescence of retinal sections for melanopsin (green), tyrosine hydroxylase (blue), and synaptic markers (red; Bassoon for left panel and CtBP2 for right panel) in both control (upper panel) and *Bax* mutant mice (lower panel). In $Bax^{-/-}$ mice, an ectopic synaptic stratum from ipRGCs and TH-amacrine cells was observed within the INL (arrowheads). (ONL, outer nucleus layer; OPL, outer plexiform layer; INL, inner nucleus layer; IPL, inner plexiform layer; GCL, ganglion cell layer). Scale bars 50 μm.
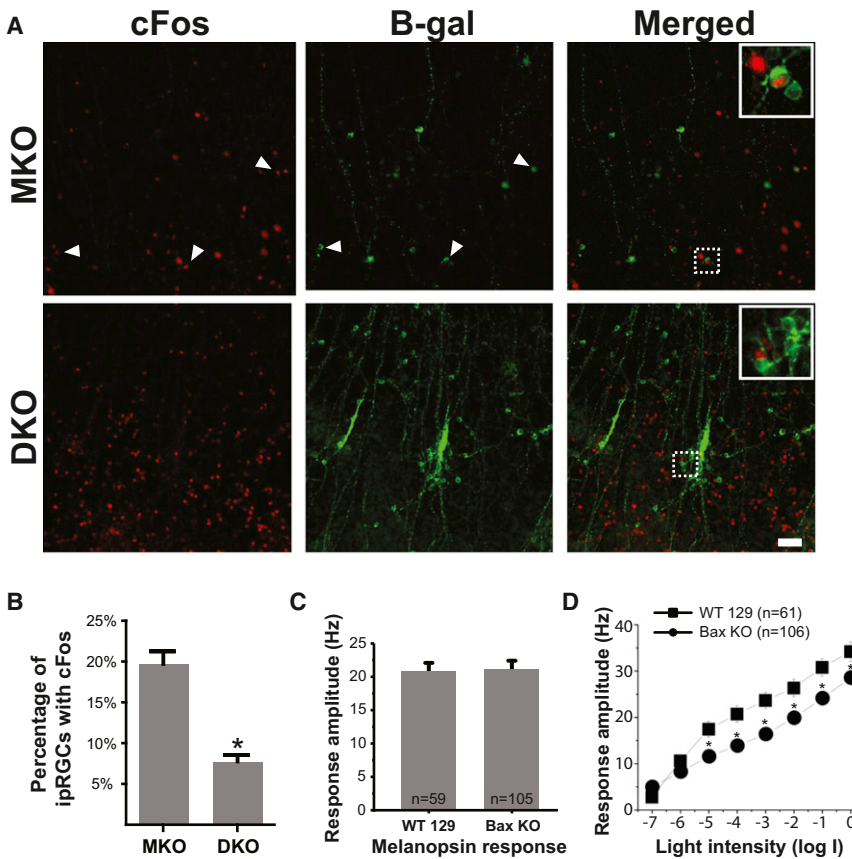
A

Figure 8. Disrupted Light Signal from Outer Retina to ipRGCs

(A) Immunofluorescence of whole-mount retina for cFos (red) and LacZ (green) in MKO ($Opn4^{tau-LacZ/tau-LacZ}$) and DKO ($Opn4^{tau-LacZ/tau-LacZ}$; $Bax^{-/-}$) mice after 30 min of light exposure. No cFos activation was observed within clumped ipRGCs in DKO mice. Scale bars, 50 μm.

(B) Quantification of cFos positive ipRGCs after 30 min of light exposure. DKO mice show a significantly lower percentage of cFos positive ipRGCs than MKO mice.

(C) Electrophysiological recording of melanopsin response from ipRGCs under the synaptic blocker cocktail from both control and Bax mutant mice at intensity = −0 log I.

(D) Electrophysiological recording of ipRGCs spike frequency under various light intensities using multielectrode array. Light response from ipRGCs in $Bax^{-/-}$ mice is significantly weaker across different light intensities. ipRGCs were identified after application of the synaptic blocker cocktail (* indicates p < 0.05 by t test, mean ± SEM).

within the INL (Figure 7A, labeled red) that receives ON synaptic input from bipolar cells (Figure 7B). Specifically, there is an increase in the number of ectopic ON synapses within the INL in $Bax^{-/-}$ animals compared to controls, whereas, surprisingly, the number of en passant ON synapses, normally observed between ON-bipolar cells and ipRGCs in S1 of the inner plexiform layer (IPL) (Dumitrescu et al., 2009), remains exactly the same (Figure 7C). We further investigated the colocalization of a synaptic partner of ipRGCs, the dopaminergic amacrine cell, which normally co-stratifies with ipRGCs in the outermost stratum S1 of the IPL (Zhang et al., 2008; Matsuoka et al., 2011; Figure 7A, bottom panels, labeled blue). In the $Bax^{-/-}$ retina, such dopaminergic processes are also mislocalized to the ectopic synaptic layer embedded within the INL (Figure 7A, bottom panels). ipRGCs, therefore, are not only disrupted in their spacing, but also show abnormalities in the distribution of their dendrites across the depth of the retina and in the location of their synaptic contacts with ON bipolar and dopaminergic amacrine cells. These morphological and behavioral data from Bax mutant animals strongly indicate that the Bax mutation causes disruptions in normal ipRGC circuitry within the retina.

To directly determine whether rod/cone signaling to ipRGCs in the retina was altered in $Bax^{-/-}$ animals, we assessed light dependent retinal activation of ipRGCs by performing cFos immunostaining in $Bax^{-/-}$ animals that also lack the melanopsin protein. Specifically, we colabeled cFos and ipRGCs using double immunofluorescence with beta-galactosidase as a marker for ipRGCs in whole-mount retinas from $Opn4^{tau-LacZ/tau-LacZ}$ mice and $Bax^{-/-}$; $Opn4^{tau-LacZ/tau-LacZ}$ mice. In $Opn4^{tau-LacZ/tau-LacZ}$ mice, 20% of ipRGCs showed detectable cFos staining after 30 min of light exposure. In contrast, in $Bax^{-/-}$; $Opn4^{tau-LacZ/tau-LacZ}$ double-mutant mice, only 10% of ipRGCs showed cFos staining under the same light conditions (Figures 8A and 8B). No cFos staining was detected in clumped ipRGCs (inset in Figure 8A bottom right panel). These results indicate that outer retinal signaling to ipRGCs is diminished in the $Bax^{-/-}$ mice.

To quantitatively analyze the deficits in rod/cone input to ipRGCs, we also performed electrophysiological recordings from ipRGCs in the $Bax^{-/-}$ mice using multi-electrode array (MEA) recordings. Since we had to identify ipRGCs in the MEA recordings based on their intrinsic photosensitivity, these analyses could not be carried in $Bax^{-/-}$; $Opn4^{-/-}$ animals. We did not detect any significant differences in the intrinsic response recorded from ipRGCs from $Bax^{-/-}$ and control animals (Figure 8C), in agreement with our behavioral data that $Bax^{-/-}$ mice show normal melanopsin-dependent circadian light

(B) Double staining of ON bipolar cells (γ13) and ribbon synapses (CtBP2) shows conspicuous ON bipolar associated synapses within this ectopic synaptic region (examples are indicated by white arrows; scale bar = 20 μm).

(C) Quantification of these double-labeled synaptic profiles shows a 6-fold increase in the number of synapses in the INL in $Bax^{-/-}$ animals while the number of en passant ON synapses in S1 of the IPL, which often occur between ipRGCs and ON bipolar cells, remains the same as in controls (* indicates p < 0.001 by t test, mean ± SEM).

responses. To reveal rod/cone input, we conducted an intensity response curve starting with light intensities that are within the threshold for rod and cone responses, but are known to be subthreshold for the melanopsin intrinsic light response. We found that the ipRGCs in $Bax^{-/-}$ mice showed significantly weaker light responses compared to control animals, across several light intensities (Figure 8D). This decrement in rod/cone light input to ipRGCs is in agreement with our behavioral studies showing deficits in circadian light functions only in the absence of the melanopsin protein. Together, our morphological and functional analyses in the retina confirm that ipRGCs in the $Bax^{-/-}$ mice have deficits in relaying the rod/cone input but preserve their ability to signal light information with melanopsin photopigment.

DISCUSSION

Over the past few decades, research has shown that neurons are initially overproduced during development, only to be reduced to adult levels by programmed cell death (apoptosis). Surprisingly, in the nervous system, the elimination of Bax-mediated apoptosis results in overproduction of neurons but causes very few and only subtle functional deficits (Jonas et al., 2005; Autret and Martin, 2009; Jiao and Li, 2011). In this study, we show that apoptosis plays a critical role in generating the proper spacing and functional circuitry of ipRGCs that mediate a form of visual behavior.

The mammalian retina performs two major tasks, vision and irradiance detection (Provencio et al., 2002; Wässle, 2004). For visual functions, the orderly arrays of retinal mosaics are critical for the detection and transmission of spatial detail to central visual targets. In contrast, irradiance detection is only concerned with detecting ambient light intensity with no need for spatial resolution. The M1 ipRGCs, which predominantly contribute to irradiance detection for circadian photoentrainment and the pupillary light reflex (Chen et al., 2011), show a spaced mosaic across the retina and their dendrites form an extensive receptive net (Figure S8). Since M1 ipRGCs mediate irradiance detection, it has been assumed that their spaced distribution and uniform net of dendrites are important for enhanced photon capture (Provencio et al., 2002). In Bax mutant mice, however, lacking the regular cellular spacing and evenly distributed network of M1 ipRGCs that typify the wild-type retina, circadian light responses were indistinguishable from wild-type mice in the presence of the melanopsin protein. In contrast, Bax mutant mice were impaired in their circadian photoentrainment when only the rod/cone pathway was driving the ipRGCs. This indicates that the normal mosaic properties of M1 ipRGCs are dispensable for their intrinsic photoresponses but suggests cell spacing is required for rod/cone input.

Previous studies suggest that the dendritic arbors of M1 ipRGCs are cell-intrinsically determined, rather than being sensitive to homotypic neighbors (Lin et al., 2004). Consistent with this data, we show that the number of en passant synapses is the same in the Bax mutant mice where the number of ipRGCs is significantly increased (Figure 7C). As a consequence, disrupting ipRGC normal spacing may disrupt the uniformity of their coverage, potentially leaving regions devoid of M1 processes altogether, especially in light of the constant number of en passant synapses.

Bax mutant retinas also show abnormal fasciculation of their processes that should further exacerbate this tendency. Additionally, Bax mutant retinas show conspicuous alterations in the radial organization of the retinal synaptic architecture associated with the positioning of M1 ipRGC dendrites. These dendrites receive both increased ectopic ON input within the INL and cofasiculate with dopaminergic amacrine cells, which are also GABAergic (Contini and Raviola, 2003; Hirasawa et al., 2009). These increased ectopic synapses within the INL may lead to more inhibition of ipRGCs due to GABA release from light-activated dopaminergic amacrine cells, reducing the strength of rod/cone input to ipRGCs, which is consistent with the deficits we observed in rod/cone signaling to ipRGCs as measured by cFos activation and electrophysiological recordings (Figures 7 and 8).

It is important to note that the number of ipRGCs does not increase in the conditional Bax mutants. This is likely due to the late developmental expression of melanopsin protein (and thus also Cre recombinase in $Opn4^{Cre}$ animals) in ipRGCs, in relation to the timing of peak apoptosis (P2–P4) in RGCs. Melanopsin expression is first observed at E15 and only peaks by P3. Thus, the overlap between melanopsin-driven Cre expression and the timing of normal RGC apoptosis could result in inefficient deletion of Bax at the critical developmental period. Two testable predictions follow this hypothesis. First, in the conditional Bax mutants ($Opn4^{Cre/+}$; $Bax^{fl/fl}$), residual Bax expression in ipRGCs should still be observed at early postnatal stages. Indeed Bax antibody staining revealed residual expression in some ipRGCs (Figure S5A), in support of the first prediction. Second, using a transgenic line where Cre is expressed earlier in ipRGCs for Bax deletion in relation to apoptosis, we show better recapitulation of the $Bax^{-/-}$ phenotype. Using Math5, which is expressed in RGCs from E11–E14 (Yang et al., 2003), to drive Cre in conjunction with the floxed Bax allele ($Math5^{Cre/+}$; $Bax^{fl/fl}$), we found higher ipRGC numbers with fasciculated dendrites similar to the phenotypes seen in the conventional Bax mutants (Figure S5B). Together, these results provide strong evidence that the lack of increased cell numbers in $Opn4^{Cre/+}$; $Bax^{fl/fl}$ animals stems from the inefficiency of recombination at the Bax locus during the appropriate developmental stages. A key question that arises from our findings is why ipRGCs in the conditional Bax mutant still show disrupted spacing despite inefficient Bax deletion. The proximity-based model of how apoptosis contributes to the spaced distribution should account for this disruption: In wild-type animals, ipRGCs in close proximity undergo apoptosis, possibly by competing for limited levels of survival factors that originate in the retina and/or brain targets. In the conventional Bax knockout, all cells lack Bax and hence ipRGCs survive leading to higher cell numbers in a clumped distribution. In the conditional Bax animals, where there is stochastic Bax deletion, some ipRGCs that still retain Bax expression will be in close proximity to Bax deleted ipRGCs. This scenario will give the Bax negative ipRGCs a competitive advantage over the Bax positive ipRGCs irrespective of the survival signal. This will bias the ipRGC survival to those that lack Bax expression

including some in close proximity, thereby disrupting the regular spacing of ipRGCs in the $Opn4^{Cre/+}; Bax^{fl/fl}$ animals.

The majority of studies indicate that homotypic interactions underlie the formation of regular retinal mosaics. During the peak period of cell death at early postnatal stages, it is difficult to distinguish between the ipRGC subtypes, mainly due to the incomplete establishment of full dendritic fields. All ipRGCs express melanopsin and there are no other known markers that currently differentiate between individual subtypes. ipRGCs subtypes (M1 versus non-M1) can only be easily distinguished morphologically in adult mice by their mature dendritic fields. In our identification of apoptotic ipRGCs at P4, a caveat is that we were unable to differentiate the specific ipRGC subtypes. Thus, we cannot be certain that cells undergoing apoptosis near other ipRGCs are of the same subtype.

Interestingly, some of the phenotypes that we report here in the conventional Bax mutants, fasciculated ipRGC dendrites, disrupted mosaic spacing and increased ipRGC cell number have also been reported in mice lacking Dscam, a neuronal cell adhesion molecule (Fuerst et al., 2008, 2009). These results suggest the intriguing possibility that crosstalk between Bax and Dscam regulates proper ipRGC cell number, spacing and dendritic architecture (Keeley et al., 2012). It is also important to note that although we have assumed that the deficits observed in the Bax mutants are only apoptosis-dependent, several recent studies indicate that Bax could have roles independent of apoptosis (Jonas et al., 2005; Autret and Martin, 2009; Jiao and Li, 2011). Thus, it is feasible that some of the deficits that we observe in Bax mutants might also reflect a role for Bax in mitochondrial morphogenesis (Autret and Martin, 2009) or changes in synaptic activity (Jonas et al., 2005; Jiao and Li, 2011).

In summary, we show that Bax mutant mice exhibit conspicuous changes in the organization of the M1 ipRGC mosaic. Remarkably, none of the morphological deficits affect the intrinsic light sensitivity and transmission from the retina to the brain to control photoentrainment. This is despite the widespread assumption that a uniformly distributed network of ipRGC processes is critical for the light-gathering properties of M1 ipRGCs (Provencio et al., 2002). Indeed, for circadian photoentrainment, one might have expected the M1 population of ipRGCs to lack the properties of other regular retinal mosaics, including uniformity of their dendritic coverage across the retina, because they were originally thought to be only ambient light-sensors. With the demonstration that ipRGCs also receive direct input from ON bipolar cells relaying rod/cone input (Dumitrescu et al., 2009; Hoshi et al., 2009), it might be expected, therefore, that ipRGCs form regular mosaics similar to other RGC types, as recently demonstrated (Berson et al., 2010). Indeed, our study demonstrates a functional relevance for the M1 ipRGC mosaic in that it is crucial for the normal reception of rod/cone input to drive photoentrainment.

EXPERIMENTAL PROCEDURES

Mice

All mice were of a mixed background (C57BL/6;129SvJ), except those in Figures 1A and 1B (being congenic with C57BL/6J). Animals that were used in the behavioral analyses were between 4 and 12 months. Animals were housed and treated in accordance with NIH and IACUC guidelines, and all animal care and use protocols were approved by the Johns Hopkins University Animal Care and Use Committee. The $Math5^{cre}$ mice were a generous gift of Lin Gan. Because the cDKO and cKO lines were derived from a $Bax^{fl/fl};$ $Bak^{-/-}$ line purchased from the Jackson Laboratory (originally generated by Stanley Korsmeyer's laboratory [Takeuchi et al., 2005]), 4 out of 9 cDKO, 3 out of 7 control, and 1 out of 5 cKO mice were heterozygous for Bak ($Bak^{+/-}$) in the wheel-running activity experiments. Within each group, $Bak^{+/-}$ mice behaved no differently from $Bak^{+/+}$ mice.

Immunohistochemistry

For labeling dying cells, eyes were fixed 30 min in 4% paraformaldehyde, retinas were dissected then blocked for 2 hr in 5% goat serum, 2% donkey serum, and 0.3% Triton in 0.1 M PBS. Retinas than incubated with mouse monoclonal anti-activated Bax (1:500, 6A7 gift from Richard Youle), rabbit polyclonal anti-cleaved caspase-3 (1:200, Cell signaling), and sheep poly-clonal anti-GFP (1:500, Biogenesis) for 2 days at 4°C. Retinas were washed three time in 0.1 M PBS and then incubated with 1:800 Alexa anti-rabbit-546, anti-mouse-546, and anti-sheep-488 in blocking solution for 2 hr. After secondary antibody incubation, retinas were washed three times in 0.1 M PBS and incubated with TUNEL reaction mixture at 37°C for 1 hr according to manufacturer's instructions (in situ cell detection kit TMR red, Roche). Retinas were washed again three times in 0.1M PBS and mounted with Vectashield.

For labeling inner retinal synapses, the retinas of adult $Bax^{-/-}$ and wild-type control mice were dissected following intracardial perfusion and then either incubated in antibodies to melanopsin (a gift from Dr. Provencio), as described (Keeley et al., 2012), or they were sectioned on a vibratome and immunola-beled using antibodies to melanopsin, tyrosine hydroxylase (AB15542, Millipore), and either CtBP2 (612044, BD Transduction Laboratories) or Bassoon (VAM-PS003, Stressgen), as described (Keeley and Reese, 2010).

For labeling of ectopic synapses, retinas were dissected from whole eyes that had been fixed in 4% EM grade PFA for 20 min and cryoprotected in 30% sucrose, and 12 μm sections were taken using a cryostat. Sections were incubated in antibodies against γ13 (generously provided by Robert Margolskee) (1:500) and CtBP2 (612044, BD Transduction Laboratories) (1:250) overnight, washed, and incubated with Alexa-conjugated secondary antibodies (Invitrogen) for 3 hr.

For $cFos$ staining, mice were house in LD 12:12 and dark adapted for 2 hr prior to exposure to light for 30 min at ZT 4. After the light treatment, mice were moved to dark conditions for 1 hr. The eyes were then removed, fixed in 4% PFA for 30 min, and dissected. Retinas were fixed for additional 2 hr, blocked in 0.1 M phosphate buffer with 5% Goat serum and 0.3% Triton X-100, and then incubated with an anti-cFos antibody (Calbiochem Ab-5; 1:20,000) and an anti-beta-galactosidase antibody (Millipore; 1:2000) for 48 hr followed by incubation with Alexa-conjugated secondary antibodies (Invitrogen) for 2 hr.

Wheel-Running Activity

Wheel-running experiments were performed and analyzed similar to (Güler et al., 2008).

X-Gal Staining

Brains and retinas were prepared and stained similar to (Hattar et al., 2006).

Mosaic Analysis

One image (895 × 671 μm) was taken randomly from each of four quadrants per retina using a Zeiss microscope with Plan-Apochromat 10×/0.45 objective lens. Dots were manually placed over each individual cell body, the XY coordinates were extracted using ImageJ, fed into WinDRP program (Masland Lab), and density recovery profile (DRP) graphs were generated with a 10 μm bin size and a 10 μm cell size. Data from the four fields were averaged for each retina, and each bin in the DRP shows the mean of those retinal averages (±SEM). This cell size was chosen since the cell body of an M1 ipRGC is approximately 10 μm. The same XY coordinates were analyzed for their Voronoi tessellation of each field using specialty software to generate Voronoi domain regularity indexes (VDRI) and nearest neighbor regularity indexes

(NNRI), as previously described (Figures 5D and 5E). For all analyses, we averaged four fields per retina, and six retinas per condition, and this mean of the retinal averages (±SEM) is graphed. A similar procedure was carried out for the P0 DRP graphs and analysis of apoptosis at P4, except that we sampled a smaller area (322 × 322 μm for P0 DRP graphs and 516 × 516 μm for P4 staining) because at those developmental stages, the total retinal area is smaller. Additionally, for the analysis of apoptosis at P4, we took multiple images per quadrant to maximize our chances of analyzing apoptotic cells. Apoptotic cells that are on the periphery could not be included in our analysis. Thus, we found 77 apoptotic ipRGCs, but we were only able to analyze a fraction of these cells (39 for Voronoi domain and 44 for nearest neighbor). Voronoi domain areas and nearest neighbor distances for apoptotic and non-apoptotic ipRGCs were calculated by ImageJ and WinDRP, respectively.

In Vitro Preparation and Electrophysiological Recording

Mice of either sex and 8–12 months of age were used in these experiments. Animals were dark-adapted overnight and euthanized under dim red light with carbon dioxide. All subsequent tissue preparation procedures were performed under infrared illumination using night vision devices (NiteMate NAV-3, Litton Industries, Watertown, CT). Both eyes were harvested, hemisected, and incubated in room-temperature Ames' medium gassed with 95% O_2 5% CO_2. The retinas were isolated from the pigment epithelium and the vitreous removed from the retinas using forceps. Each retina was cut in half, and one piece was flattened on a 60-channel MEA (200/30-Ti-gr, Multi Channel Systems, Germany) with the ganglion cell side down; the other half was discarded. The retina was continuously superfused at 3 ml min^{-1} with Ames' medium gassed with 95% O_2 5% CO_2 and maintained at 33°C with a temperature controller (Warner Instruments, Hamden, CT), and was kept in darkness except when stimulated by light. Presentation of light stimuli started after the retina had been superfused for 40 min. All stimuli were 10 s full-field 480 nm light generated by a monochromator (Optical Building Blocks, Birmingham, NJ). The timing of stimulus presentation was controlled by an electromechanical shutter built into this monochromator. Light intensity was adjusted by a continuously variable neutral density filter (Newport Corporation, Franklin, MA). The intensity-adjusted light was delivered via a fiber optic cable to the retina from underneath the MEA chamber. Light intensities were calibrated using a radiometer (UDT Instruments, San Diego, CA) and the unattenuated intensity (i.e., −0 log I) was 4.1 × 10^{15} quanta cm^{-2} s^{-1} at the retina. At the end of each experiment, a pharmacological cocktail containing 50–100 μM L-(+)-2-Amino-4-phosphonobutyric acid (L-AP4), 40–80 μM 6,7-Dinitroquinoxaline-2,3-dione (DNQX), and 25 μM D-(-)-2-Amino-5-phosphonopentanoic acid (D-AP5) was applied to block rod/cone signaling to the inner retina, and ipRGCs were identified based on their ability to generate sluggish, melanopsin-based responses to −0 log I light. This cocktail completely abolished the light responses of all conventional ganglion cells (Wong et al., 2007).

Ganglion cell spiking activity was amplified, filtered with cutoffs at 200 Hz and 3 kHz, and digitized at 10 kHz using MC Rack software (Multi Channel Systems). Raw recordings from all 60 channels were saved onto a computer for offline analysis. Cluster analysis of the spike data was performed using Offline Sorter software (Plexon Inc., Dallas, TX). For Figures 8C and 8D, photoresponse amplitude was calculated by subtracting the mean firing rate during the 10 s period preceding stimulus onset from that during the 10 s light stimulus. Student t test p values were calculated using Origin software (OriginLab, Northampton, MA), with the significance level set at 0.05.

SUPPLEMENTAL INFORMATION

Supplemental Information includes eight figures, one table, and Supplemental Experimental Procedures and can be found with this article online at http://dx.doi.org/10.1016/j.neuron.2012.11.028.

ACKNOWLEDGMENTS

REFERENCES

Autret, A., and Martin, S.J. (2009). Emerging role for members of the Bcl-2 family in mitochondrial morphogenesis. Mol. Cell *36*, 355–363.

Baver, S.B., Pickard, G.E., Sollars, P.J., and Pickard, G.E. (2008). Two types of melanopsin retinal ganglion cell differentially innervate the hypothalamic suprachiasmatic nucleus and the olivary pretectal nucleus. Eur. J. Neurosci. *27*, 1763–1770.

Berson, D.M., Castrucci, A.M., and Provencio, I. (2010). Morphology and mosaics of melanopsin-expressing retinal ganglion cell types in mice. J. Comp. Neurol. *518*, 2405–2422.

Cellerino, A., Galli-Resta, L., and Colombaioni, L. (2000). The dynamics of neuronal death: a time-lapse study in the retina. J. Neurosci. *20*, RC92.

Chen, S.K., Badea, T.C., and Hattar, S. (2011). Photoentrainment and pupillary light reflex are mediated by distinct populations of ipRGCs. Nature *476*, 92–95.

Contini, M., and Raviola, E. (2003). GABAergic synapses made by a retinal dopaminergic neuron. Proc. Natl. Acad. Sci. USA *100*, 1358–1363.

Cook, J.E. (1998). Getting to grips with neuronal diversity: What *is* a neuronal type? In Development and Organization of the Retina, L. Chalupa and B. Finlay, eds. (New York: Plenum Press), pp. 91–120.

Cook, J.E., and Chalupa, L.M. (2000). Retinal mosaics: new insights into an old concept. Trends Neurosci. *23*, 26–34.

Dreher, B., Potts, R.A., and Bennett, M.R. (1983). Evidence that the early postnatal reduction in the number of rat retinal ganglion cells is due to a wave of ganglion cell death. Neurosci. Lett. *36*, 255–260.

Dumitrescu, O.N., Pucci, F.G., Wong, K.Y., and Berson, D.M. (2009). Ectopic retinal ON bipolar cell synapses in the OFF inner plexiform layer: contacts with dopaminergic amacrine cells and melanopsin ganglion cells. J. Comp. Neurol. *517*, 226–244.

Ecker, J.L., Dumitrescu, O.N., Wong, K.Y., Alam, N.M., Chen, S.-K., LeGates, T., Renna, J.M., Prusky, G.T., Berson, D.M., and Hattar, S. (2010). Melanopsin-expressing retinal ganglion-cell photoreceptors: cellular diversity and role in pattern vision. Neuron *67*, 49–60.

Farah, M.H., and Easter, S.S., Jr. (2005). Cell birth and death in the mouse retinal ganglion cell layer. J. Comp. Neurol. *489*, 120–134.

Freedman, M.S., Lucas, R.J., Soni, B., von Schantz, M., Muñoz, M., David-Gray, Z., and Foster, R. (1999). Regulation of mammalian circadian behavior by non-rod, non-cone, ocular photoreceptors. Science *284*, 502–504.

Fuerst, P.G., Koizumi, A., Masland, R.H., and Burgess, R.W. (2008). Neurite arborization and mosaic spacing in the mouse retina require DSCAM. Nature *451*, 470–474.

Fuerst, P.G., Bruce, F., Tian, M., Wei, W., Elstrott, J., Feller, M.B., Erskine, L., Singer, J.H., and Burgess, R.W. (2009). DSCAM and DSCAML1 function in self-avoidance in multiple cell types in the developing mouse retina. Neuron *64*, 484–497.

Galli-Resta, L. (2002). Putting neurons in the right places: local interactions in the genesis of retinal architecture. Trends Neurosci. *25*, 638–643.

Güler, A.D., Ecker, J.L., Lall, G.S., Haq, S., Altimus, C.M., Liao, H.-W., Barnard, A.R., Cahill, H., Badea, T.C., Zhao, H., et al. (2008). Melanopsin cells are the principal conduits for rod-cone input to non-image-forming vision. Nature 453, 102–105.

Hattar, S., Liao, H.W., Takao, M., Berson, D.M., and Yau, K.W. (2002). Melanopsin-containing retinal ganglion cells: architecture, projections, and intrinsic photosensitivity. Science 295, 1065–1070.

Hattar, S., Lucas, R.J., Mrosovsky, N., Thompson, S., Douglas, R.H., Hankins, M.W., Lem, J., Biel, M., Hofmann, F., Foster, R.G., and Yau, K.-W. (2003a). Melanopsin and rod-cone photoreceptive systems account for all major accessory visual functions in mice. Nature 424, 76–81.

Hattar, S., Lucas, R.J., Mrosovsky, N., Thompson, S., Douglas, R.H., Hankins, M.W., Lem, J., Biel, M., Hofmann, F., Foster, R.G., and Yau, K.W. (2003b). Melanopsin and rod-cone photoreceptive systems account for all major accessory visual functions in mice. Nature 424, 76–81.

Hattar, S., Kumar, M., Park, A., Tong, P., Tung, J., Yau, K.W., and Berson, D.M. (2006). Central projections of melanopsin-expressing retinal ganglion cells in the mouse. J. Comp. Neurol. 497, 326–349.

Hirasawa, H., Puopolo, M., and Raviola, E. (2009). Extrasynaptic release of GABA by retinal dopaminergic neurons. J. Neurophysiol. 102, 146–158.

Hoshi, H., Liu, W.L., Massey, S.C., and Mills, S.L. (2009). ON inputs to the OFF layer: bipolar cells that break the stratification rules of the retina. J. Neurosci. 29, 8875–8883.

Jiao, S., and Li, Z. (2011). Nonapoptotic function of BAD and BAX in long-term depression of synaptic transmission. Neuron 70, 758–772.

Jonas, E.A., Hardwick, J.M., and Kaczmarek, L.K. (2005). Actions of BAX on mitochondrial channel activity and on synaptic transmission. Antioxid. Redox Signal. 7, 1092–1100.

Keeley, P.W., and Reese, B.E. (2010). Morphology of dopaminergic amacrine cells in the mouse retina: independence from homotypic interactions. J. Comp. Neurol. 518, 1220–1231.

Keeley, P.W., Sliff, B.J., Lee, S.C., Fuerst, P.G., Burgess, R.W., Eglen, S.J., and Reese, B.E. (2012). Neuronal clustering and fasciculation phenotype in Dscam- and Bax-deficient mouse retinas. J. Comp. Neurol. 520, 1349–1364.

Lin, B., Wang, S.W., and Masland, R.H. (2004). Retinal ganglion cell type, size, and spacing can be specified independent of homotypic dendritic contacts. Neuron 43, 475–485.

Lobe, C.G., Koop, K.E., Kreppner, W., Lomeli, H., Gertsenstein, M., and Nagy, A. (1999). Z/AP, a double reporter for cre-mediated recombination. Dev. Biol. 208, 281–292.

Lucas, R.J., Douglas, R.H., and Foster, R.G. (2001). Characterization of an ocular photopigment capable of driving pupillary constriction in mice. Nat. Neurosci. 4, 621–626.

Lucas, R.J., Hattar, S., Takao, M., Berson, D.M., Foster, R.G., and Yau, K.-W. (2003). Diminished pupillary light reflex at high irradiances in melanopsin-knockout mice. Science 299, 245–247.

Matsuoka, R.L., Nguyen-Ba-Charvet, K.T., Parray, A., Badea, T.C., Chédotal, A., and Kolodkin, A.L. (2011). Transmembrane semaphorin signalling controls laminar stratification in the mammalian retina. Nature 470, 259–263.

McNeill, D.S., Sheely, C.J., Ecker, J.L., Badea, T.C., Morhardt, D., Guido, W., and Hattar, S. (2011). Development of melanopsin-based irradiance detecting circuitry. Neural Dev. 6, 8.

Mosinger Ogilvie, J., Deckwerth, T.L., Knudson, C.M., and Korsmeyer, S.J. (1998). Suppression of developmental retinal cell death but not of photoreceptor degeneration in Bax-deficient mice. Invest. Ophthalmol. Vis. Sci. 39, 1713–1720.

Mrosovsky, N., and Hattar, S. (2003). Impaired masking responses to light in melanopsin-knockout mice. Chronobiol. Int. 20, 989–999.

Novak, A., Guo, C., Yang, W., Nagy, A., and Lobe, C.G. (2000). Z/EG, a double reporter mouse line that expresses enhanced green fluorescent protein upon Cre-mediated excision. Genesis 28, 147–155.

Panda, S., Sato, T.K., Castrucci, A.M., Rollag, M.D., DeGrip, W.J., Hogenesch, J.B., Provencio, I., and Kay, S.A. (2002). Melanopsin (Opn4) requirement for normal light-induced circadian phase shifting. Science 298, 2213–2216.

Perry, V.H., Henderson, Z., and Linden, R. (1983). Postnatal changes in retinal ganglion cell and optic axon populations in the pigmented rat. J. Comp. Neurol. 219, 356–368.

Provencio, I., Rollag, M.D., and Castrucci, A.M. (2002). Photoreceptive net in the mammalian retina. This mesh of cells may explain how some blind mice can still tell day from night. Nature 415, 493.

Raven, M.A., Eglen, S.J., Ohab, J.J., and Reese, B.E. (2003). Determinants of the exclusion zone in dopaminergic amacrine cell mosaics. J. Comp. Neurol. 461, 123–136.

Reese, B.E. (2008). Mosaic architecture of the mouse retina. In Eye, Retina, and Visual Systems of the Mouse, L.M. Chalupa and R.W. Williams, eds. (Cambridge: MIT Press), pp. 147–155.

Ruby, N.F., Brennan, T.J., Xie, X., Cao, V., Franken, P., Heller, H.C., and O'Hara, B.F. (2002). Role of melanopsin in circadian responses to light. Science 298, 2211–2213.

Schmidt, T.M., and Kofuji, P. (2009). Functional and morphological differences among intrinsically photosensitive retinal ganglion cells. J. Neurosci. 29, 476–482.

Takeuchi, O., Fisher, J., Suh, H., Harada, H., Malynn, B.A., and Korsmeyer, S.J. (2005). Essential role of BAX,BAK in B cell homeostasis and prevention of autoimmune disease. Proc. Natl. Acad. Sci. USA 102, 11272–11277.

Viney, T.J., Balint, K., Hillier, D., Siegert, S., Boldogkoi, Z., Enquist, L.W., Meister, M., Cepko, C.L., and Roska, B. (2007). Local retinal circuits of melanopsin-containing ganglion cells identified by transsynaptic viral tracing. Curr. Biol. 17, 981–988.

Wässle, H. (2004). Parallel processing in the mammalian retina. Nat. Rev. Neurosci. 5, 747–757.

White, F.A., Keller-Peck, C.R., Knudson, C.M., Korsmeyer, S.J., and Snider, W.D. (1998). Widespread elimination of naturally occurring neuronal death in Bax-deficient mice. J. Neurosci. 18, 1428–1439.

Wong, K.Y., Dunn, F.A., Graham, D.M., and Berson, D.M. (2007). Synaptic influences on rat ganglion-cell photoreceptors. J. Physiol 582, 279–296.

Yang, Z., Ding, K., Pan, L., Deng, M., and Gan, L. (2003). Math5 determines the competence state of retinal ganglion cell progenitors. Dev. Biol. 264, 240–254.

Zhang, D.Q., Wong, K.Y., Sollars, P.J., Berson, D.M., Pickard, G.E., and McMahon, D.G. (2008). Intraretinal signaling by ganglion cell photoreceptors to dopaminergic amacrine neurons. Proc. Natl. Acad. Sci. USA 105, 14181–14186.